Oxygen Hole States in Zirconia Lattices: Quantitative Aspects of Their Cathodoluminescence Emission

ARTICLE *in* THE JOURNAL OF PHYSICAL CHEMISTRY A · SEPTEMBER 2014

Impact Factor: 2.69 · DOI: 10.1021/jp506923p · Source: PubMed

THE JOURNAL OF PHYSICAL CHEMISTRY A

Article

pubs.acs.org/JPCA

Oxygen Hole States in Zirconia Lattices: Quantitative Aspects of Their Cathodoluminescence Emission

M. Boffelli,[†] W. Zhu,[†] M. Back,[‡] G. Sponchia,[‡] T. Francese,[‡] P. Riello,[‡] A. Benedetti,[‡] and G. Pezzotti*[,†]

[†]Kyoto Institute of Technology and Research Institute for Nanoscience, Sakyo-ku, Matsugasaki, 606-8585 Kyoto, Japan

[‡]Department of Molecular Sciences and Nanosystems, Ca' Foscari University of Venice, Dorsoduro 2137, 30123 Venezia, Italy

ABSTRACT: Systematic assessments of cathodoluminescence (CL) spectroscopy, Raman spectroscopy (RS), and X-ray diffraction (XRD) are presented for pure zirconia and for a series of Y-doped zirconia powders (henceforth, simply referred to as undoped ZrO_2 and YSZ powders, respectively) synthesized according to a coprecipitation method of Zr and Y chlorides. Emphasis is placed here on spectral emissions related to oxygen-vacancy sites (i.e., oxygen hole states) equally detected from undoped and Y-doped ZrO_2 samples, either as intrinsic defects or, extrinsically induced, by means of cathodoluminescence. Most counterintuitively, the undoped ZrO_2 sample (i.e., the one with presumably the lowest amount of oxygen vacancies) experienced the strongest CL emission. A progressive "quenching" effect on CL emission with increasing the fraction of Y^{3+} dopant could also be observed because the intrinsic vacancies present in the undoped lattice are the most efficient since they can trap two electrons to gain electrical neutrality. However, as soon as Y^{3+} ions are introduced in the system, those intrinsic vacancies migrate to Y-sites in next-nearest-neighbor locations, namely in a less efficient lattice location. This phenomenon is tentatively referred to as "delocalization" of vacancy sites. Moreover, the fact that Y-doped zirconia series presents quite similar CL spectra compared to the undoped zirconia could be an evidence that the radiative centers of undoped and Y-doped ZrO_2 are basically the same. A fitting procedure has been made aiming to give a rational description of the variation of the spectra morphology, and a parameter able to describe the monoclinic to tetragonal phase transformation has been found. This parameter and the overall set of CL data enabled us to quantitatively assess polymorphic phase fractions by CL spectroscopy in the scanning electron microscope.

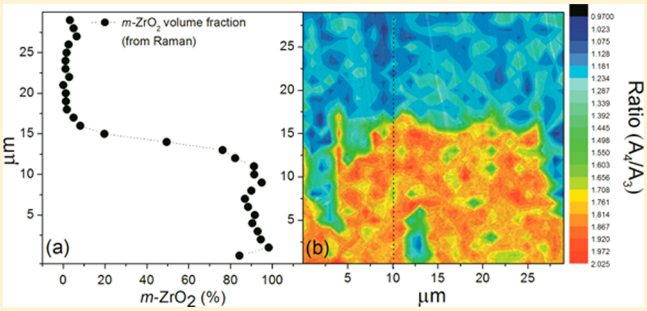

1. INTRODUCTION

Detailed understanding of the structure and off-stoichiometry of oxygen sublattice in ionic materials and its mobility/stability under different environmental conditions is a key to solve a number of fundamentally important technological problems. These (nonexhaustively) include designing biomedical devices made of oxide ceramics with significantly improved lifetimes in the human body,[1−3] improving dielectric permittivity in oxynitride relaxor-type ferroelectrics with perovskitic structure,[4] and enhancing ionic conductivity in fuel cell electrolytes.[5] In all these cases, anion order is expected to have a strong influence on physical properties, especially when these are sensitive to local disorder and distortions.[6] In this context, cathodoluminescence spectroscopy (CL) has already been phenomenologically applied to a number of advanced topics and appears to possess a potential to unfold several fundamental issues to them related.[7−11] Besides its uniqueness as a direct means of visualizing oxygen vacancy concentration in the very neighborhood of oxide surfaces, CL is also capable of providing mechanical stress information by exploiting a piezo-spectroscopic effect on the light emission from oxygen vacancy sites. In other words, the vacancy sites can be employed, upon preliminary quantitative calibrations, as "stress sensors" in both crystalline and amorphous lattices.[8−10,12] However, many basic aspects of the CL emission from oxide materials yet remain to be clarified, which confines CL spectroscopy to somewhat incomplete outputs and limits its potential efficacy both in material physics and in applicative engineering research.

Oxygen vacancies can have a significant role in defining the functional and structural properties of ZrO_2 ceramics. For example, their concentration and spatial distribution are decisive factors in environmental stability and ionic diffusivity. Actively doping ZrO_2 with aliovalent cations (e.g., Y^{3+}, Mg^{2+}), for example, is a known approach to partially stabilize the tetragonal phase at room temperature,[7,13−15] a practice that has widely been put into use in designing oxide materials for biomedical devices. Nitrogen anions can also be introduced in the ZrO_2 lattice upon annealing under pressure to partially replace oxygen in solid electrolytes under reducing conditions.[16] An example is the adsorption/hydroxylation of water at vacancy sites on environmentally exposed ZrO_2 surfaces. In previous papers,[7,13] we have accurately monitored

Received: July 11, 2014
Revised: August 29, 2014
Published: September 26, 2014

dx.doi.org/10.1021/jp506923p | J. Phys. Chem. A 2014, 118, 9828−9836

the oxygen-vacancy activity of ZrO_2-related ceramics, as well as that of other ceramic oxides like as Al_2O_3 and TiO_2, by means of spectrally and spatially resolved CL spectroscopy. However, compared to other ionic solids, the CL behavior of zirconia is definitely more cryptic and counterintuitive. The most striking feature we have found is that the intensity of the CL signal emitted from a substoichiometric YSZ lattice actually decreases with increasing oxygen-vacancy concentration. Note that, if the CL signal were directly emitted from the oxygen-vacancy site, one would expect that its intensity should increase, rather than decrease, with increasing vacancy concentration. This effect, already reported by several different research groups,[17−19] has not yet been unambiguously explained, although several interpretations have been offered in the attempt to elucidate it. Moreover, oxygen vacancies introduce localized band gap states in ZrO_2, resulting in several distinct (but partially overlapping) CL emission bands. These bands have been interpreted as energetically differentiated owing to morphological details of the vacancy site in the presence of substitutional Y^{3+} cations (i.e., the Y^{3+} ion being either nearest neighbor or next-nearest neighbor to the vacancy).[20] However, the same CL bands also appear (and more strongly) in undoped ZrO_2. Theoretical studies,[21−23] carried out on substoichiometric ZrO_2, have examined the stability of both bulk and surface defects in its different polymorphic structures. These studies are quite useful and might provide us with a guide to interpret the CL emission arising from oxygen hole states in the ZrO_2 lattices, in light of the experimental program newly carried out on powder samples in our study here.

This paper is aimed at improving understanding of the CL behavior of ZrO_2 and at establishing some yet phenomenological, but otherwise quantitative, aspects of its CL emission, which could be useful in materials science assessments. It is shown that advancing the physics behind the CL emission of ZrO_2 might open the way to polymorphic fractions in the scanning electron microscope. Therefore, it follows that such assessments could be pursued exploiting electron excitation rather than laser beams, with a so far unachieved spatial resolution.

2. THEORETICAL BASES

The CL emission from the yttria-stabilized ZrO_2 lattice consists of a main broad band, which has been reported to represent the sum of distinct emissions from oxygen-related defects with different structures.[20] The overall broad band (peaking at around 500 nm) has been interpreted (with some general consensus) as being contributed by three partially overlapping sub-bands of Gaussian nature located at around 460 nm (2.69 eV), 550 nm (2.25 eV), and 600 nm (2.07 eV). The emission at 460 nm (also referred to as the F^+ center of ZrO_2) is attributed to singly occupied anion vacancies, thus involving the presence of an intrinsic defect site, in which all Zr ions are nearest neighbors to the vacancy. The two additional sub-bands, located at 550 and 600 nm (i.e., usually referred to as F_A^+ and F_{AA}^+ centers, respectively), were also associated with electron transfer from the valence band to local midgap states. Their structures were interpreted as consisting of one and two Y^{3+} ions as nearest neighbors to the vacancy, respectively.[21,22,24,25] A schematic of the structure of different vacancy sites and of the associated oxygen-hole electronic transitions are shown in Figure 1.

With this background in mind, the (only) starting point of our investigation will be that the intensity of the above-

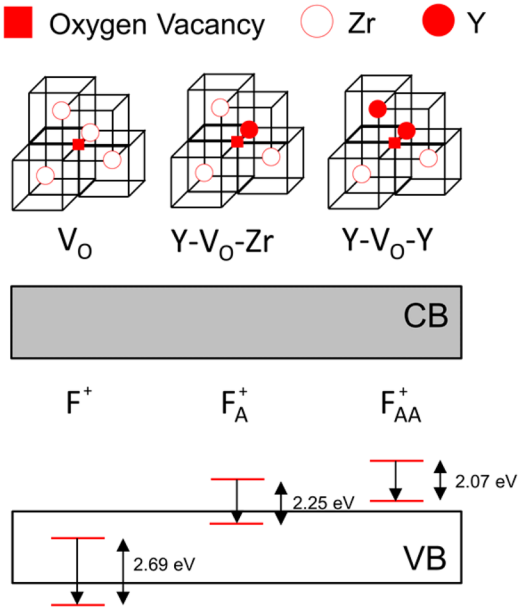

Figure 1. Simplified schemes of different vacancy sites in yttria-stabilized ZrO_2 (after ref 27).

described CL emission should actually be related to the presence of vacancy sites in the ZrO_2 lattice. In other words, what we actually observe in the visible range of the CL spectrum is clearly the final result of the intra-band-gap activity of an oxygen-deficient sublattice. However, we also argue that, since vacancy annihilation (rather than vacancy formation) leads to an increase of CL intensity in ZrO_2 ceramics, it cannot be (only) the concentration of oxygen holes themselves that determines the intensity of the CL emission, but some other intrinsic factor directly or indirectly associated with its efficiency. One way to explain the increase of CL intensity, associated with oxygen vacancy annihilation, has been to infer the emission as only occurring from an intrinsic vacancy site in the presence of a heavily strained lattice.[26] We shall henceforth refer this possibility to as the "strained-lattice hypothesis". Being the efficiency of the CL intensity directly related to Zr−O bond stretching and owing to the fact that an increased presence of oxygen vacancies redistributes the highly localized lattice strain, the higher the vacancy concentration, the lower the CL emission intensity. This would mean that a highly strained lattice is more efficient in its emission at oxygen vacancy sites. Another way to interpret the phenomenon is to foresee oxygen vacancies acting as charge traps and suppressing charge (and possibly also energy transfer). The strongest argument in favor of this interpretation is that irradiation by laser (i.e., within the band gap) directly excites the defects and results in an increase in luminescence emission with increasing oxygen vacancies for those very same samples for which a decrease in CL emission is recorded.[17,27] The electron beam creates high-energy excitations in the crystal structure, and relaxation of these excitations shall result in an extensive appearance of electrons in the conductivity band and holes in the valence band. It is expected that, under the highly energetic excitation of an electron beam, most of the luminescence centers be activated. A decrease in CL intensity under electron excitation shows that oxygen vacancies actually disturb energy transfer to the electronic transition responsible for luminescence emission. If this is the case, oxygen vacancies might act as

dx.doi.org/10.1021/jp506923p | J. Phys. Chem. A 2014, 118, 9828−9836

charge traps, thereby decreasing the number of available electrons; the more numerous the vacancy sites, the lower the CL intensity. This hypothesis will henceforth be referred to as the "charge-trap hypothesis".

In the remainder of this paper, we shall show our attempts to experimentally test the two different hypotheses mentioned above, in order to clarify the anomalous behavior of the oxygen hole states in the ZrO_2 lattice. At the outset, however, we shall notice that, unlike the interpretation under the strained-lattice hypothesis, if charge trap actually is the origin of the anomalous CL behavior of ZrO_2, this phenomenon should be independent of the polymorphic state of the lattice. On the other hand, if the strain-lattice hypothesis holds, the polymorphic state will matter; the more the oxygen vacancies in a given polymorph, the higher the amount of strain relaxation in the lattice and the lower the CL intensity.

3. EXPERIMENTAL METHOD

Undoped zirconia and a set of $Zr_{1-x}Y_xO_{2-(x/2)}$ (YSZ) powders were synthesized according to a coprecipitation method. The sample preparation procedure has extensively been described elsewhere,[28] but it is briefly repeated here. The precursor used for obtaining zirconia powder was zirconyl chloride octahydrate ($ZrOCl_2$) (Aldrich, 98%), while yttrium(III) chloride hexahydrate (Aldrich, 99.9%) was added to it for obtaining a series of nonstoichiometric $Zr_{1-x}Y_xO_{2-(x/2)}$ powders. The powder preparation procedure consisted of the following steps: (i) preparation of mixed solutions in ethanol solvent of the two precursors with appropriate Y^{3+}/Zr^{4+} ratios; (ii) addition of ammonia to the mixed solutions, which resulted in the coprecipitation of the desired compound; (iii) washing the coprecipitated powder first with water and then with ethanol; and (iv) calcining at 1000 °C in air for 12 h. By varying the ratio Y^{3+}/Zr^{4+}, it was possible to obtain a number of YSZ powder samples (labeled with different nominal amounts of oxygen vacancies). The calculated stoichiometry for those synthesized compounds is reported in Table 1. The average particle size for all the synthesized powders was around 100 nm. The undoped sample was labeled ZrO_2, while the series of eight YSZ samples were labeled *n*-YSZ, with the initial number corresponding to the percent (nominal) molar fraction of substitutional Y^{3+} ions.

Table 1. Stoichiometric Composition of the Obtained $Zr_xY_yO_z$ Powders

sample	Zr (x)	Y (y)	O (z)
ZrO_2	1		2
1-YSZ	0.990	0.010	1.995
3-YSZ	0.970	0.030	1.985
4-YSZ	0.960	0.040	1.980
4.5-YSZ	0.955	0.045	1.978
5-YSZ	0.950	0.050	1.975
8-YSZ	0.920	0.080	1.960
12-YSZ	0.880	0.120	1.940
20-YSZ	0.800	0.200	1.900

CL spectroscopy was performed inside the chamber of a field-emission-gun scanning electron microscope (FEG-SEM), equipped with an Schottky-emission type gun (S-4300SE, Hitachi, Tokyo, Japan) as the excitation source. The acceleration voltage was set at 5 kV, and the probe current was fixed at 180 pA. These conditions were rigorously maintained throughout all the experiments. A high-sensitivity CL detector unit (MP-32FE, Horiba Ltd., Kyoto, Japan) was employed for the collection of CL emission upon reflection into an ellipsoidal mirror and transmission through a bundle of optical fibers, using a high-resolution monochromator (TRIAX 320, Jobin-Ivon-Spex, Kyoto, Japan) equipped with a nitrogen-cooled 1024 × 256 pixel CCD camera (CCD-3500 V, Horiba Ltd., Kyoto, Japan). A grating of 150 grooves mm^{-1} was used throughout all the experiments. Integration time was 10 s, and the electron beam spot size was 500 nm. Average spectra were computed from 20 randomly collected spectra on each of the investigated samples. The ZrO_2 sample and the 1−20 YSZ series were sputtered with 10 nm of platinum coating and fixed with carbon tape to an aluminum sample holder.

A Philips diffractometer with a PW 1319 goniometer with Bragg−Brentano geometry, connected to a highly stabilized generator (40 kV), was used for the XRPD measurements. A focusing graphite monchromator and a proportional counter with a pulse-height discriminator were used. Nickel-filtered Cu Kα radiation and a step-by-step technique were employed (steps of 0.05, 2 h), with collection times of 10 s per step. The quantitative phase analysis by X-ray diffration was performed using the Rietveld method (DBWS9600 computer program written by Sakthivel and Young and modified by Riello et al.[29]).

Raman spectra were collected from different areas randomly selected on the samples. All spectra were taken at room temperature using a triple monochromator (T-64000, Jobin-Ivon/Horiba Group, Kyoto, Japan) equipped with a charge-coupled device (CCD) detector and analyzed by using commercially available software (Labspec, Horiba/Jobin-Yvon, Kyoto, Japan). A confocal configuration of the Raman probe was adopted throughout all the experiments, which involved the use of a 100× objective lens.

Quantitative calculation of the monoclinic volume fraction has been made from Raman spectroscopy data using eq 1 proposed by Katagiri et al.[30]

$$V_m = \frac{\frac{1}{2}(I_m^{181} + I_m^{182})}{kI_t^{148} + \frac{1}{2}(I_m^{181} + I_m^{182})} \quad (1)$$

where k is a correcting factor of the difference of scattering cross section between the monoclinic bands (181 and 192 cm^{-1}) and tetragonal band (145 cm^{-1}).

4. RESULTS AND DISCUSSION

4.1. RS and XRD Results. Both X-ray diffractometry and Raman spectroscopy data confirmed that the synthesis route actually generated different ZrO_2 polymorphs in the synthesized powders. Figure 2 shows the detected Raman spectra for all the synthesized powders. In Figure 2, all the Raman bands are labeled with using M, T, and C for indicating their belonging to the monoclinic, the tetragonal, and the cubic polymorph, respectively. The monoclinic symmetry is distinguishable by 18 Raman peaks corresponding to 18 active modes, while the tetragonal one (obtained in the case through Y^{3+} substitution for Zr^{4+}) possesses only 6 Raman-active modes.[31,32] In this study, only the undoped ZrO_2 sample possessed a fully monoclinic structure, while the samples 1-YSZ and 3-YSZ incorporated a negligible but not zero amount of tetragonal polymorph. In the range between 3 and 5 at. % of yttrium-doped powders a mixture of monoclinic and tetragonal polymorphs was clearly observed. Above 5 and up to 12 at. % of Y^{3+}, the structure resulted in a fully tetragonal symmetry, and

dx.doi.org/10.1021/jp506923p | J. Phys. Chem. A 2014, 118, 9828−9836

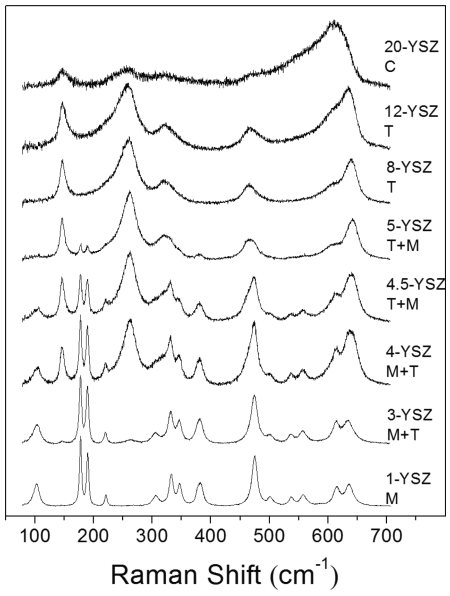

Figure 2. Raman spectra of YSZ samples as a function of dopant content.

finally for Y^{3+} contents of 20 at. %, the structure was found to be fully cubic.

These results were in full agreement with the ones obtained from Rietveld analysis of the various YSZ diffraction patterns, as shown in Figure 3a. In Figure 3b, monoclinic and tetragonal volume fractions are shown against the content of Y^{3+}. The synthesized samples showed almost the same morphology of the crystallites for all the different compositions, the average diameter of the quasi-spherical particles being ∼100 nm. This circumstance allowed us to obtain comparable results, owing to the well-known dependence of peak position and band shape of luminescence on particle size at the nanometer scale.[33,34]

4.2. CL Results. The CL emission of the samples was measured with irradiating the samples with electron excitation energies of 5 and 8 kV. Since irradiation with 5 and 8 kV basically led to identical results, only the CL results obtained with 5 kV irradiation are henceforth reported. Note that the adopted excitation energy exceeds the band-gap energies of both undoped and Y-doped ZrO_2. However, given the quite low efficiency of the band-gap emission, we could not directly detect it in any of the samples investigated. Excitation by electrons led to the formation of electron−hole pairs, which could be trapped in different metastable energy states within the band gap. Different energy states were thus generated at different defect sites in the polymorphic structures of the synthesized samples. The broad luminescence emission, which was in line with previous reports,[7,8,13] was indeed the result of overlapping sub-bands, each one arising from differently structured defective centers. In order to obtain a better understanding of the luminescence mechanisms, we attempted a fitting procedure to deconvolute the obtained CL spectra, according to previous literature.[11,13] A set of six Gaussian bands has been used (for both undoped ZrO_2 and YSZ samples) with positions and full width at half-maximum fixed only for the YSZ samples. This fitting procedure has been made aiming to give a rational description of the variation of the spectra morphology, taking into account previous findings in the literature. A comparison between deconvoluted spectra of what we could define here as our "standard" CL spectrum for different polymorphs under 5 kV electron irradiations is shown in Figures 4a, 4b, and 4c, as obtained for selected YSZ samples only consisting of monoclinic, tetragonal, and cubic polymorphs, respectively. These spectra refer to YSZ samples with 1, 8, and 20 at. % of Y^{3+}, respectively.

The CL spectra obtained under exactly the same experimental conditions for the undoped ZrO_2 sample and for the overall set of YSZ systems are reported in Figures 5 and 6, respectively. Peak positions, widths, and relative intensities in the respective (normalized) emission spectra of the Gaussian sub-bands are reported in Table 2.

Although at a first glance all the recorded spectra might look similar, the above-mentioned fitting procedure revealed fundamental differences in the spectrum morphology.

Let us start considering the emission of the undoped zirconia; as shown in Figure 5, the sample possesses a quite strong cathodoluminescence emission. The broad luminescence band observed is generated from a set of metastable energy levels, corresponding to different type of intrinsic oxygen vacancies, which are present within the band gap,[35] although the presence of some impurities in the precursor could also generate luminescence emission. Unfortunately, the precursor used in this case contained a small amount of hafnia (HfO_2). Usually, the presence of Hf^{4+} is quite common even in highly pure undoped ZrO_2 samples, and the substitution of this cation to Zr^{4+} generates a luminescence emission around 1.7 eV.[36,37] Taking this into account, we ascribed the (weaker) band (labeled Z6 and A6 respectively in Figures 5 and 6) founded at higher wavelengths around 700 nm to the oxygen vacancy luminescence emission in HfO_2.

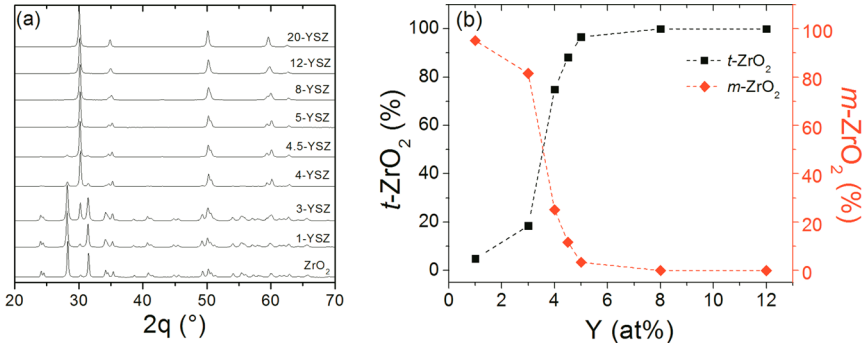

Figure 3. XRD patterns of YSZ samples (a) and calculated monoclinic and tetragonal volume fraction from Rietveld refinement (b) as a function of dopant content.

dx.doi.org/10.1021/jp506923p | J. Phys. Chem. A 2014, 118, 9828−9836

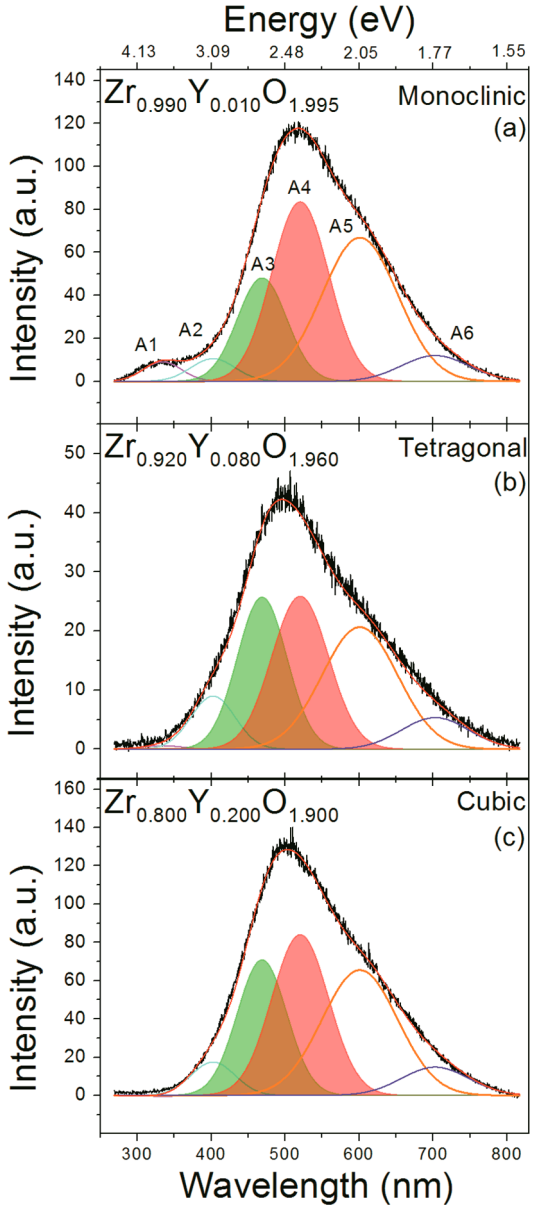

Figure 4. CL spectra of the monoclinic 1-YSZ (a), tetragonal 8-YSZ (b), and cubic 20-YSZ (c) samples with the relative Gaussian line-shape fitted bands.

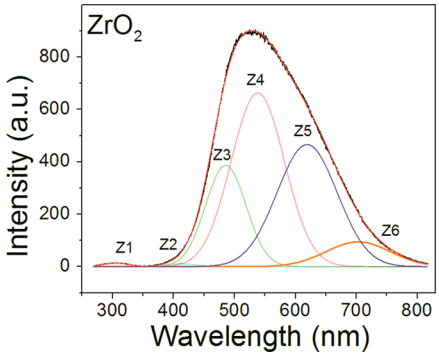

Figure 5. Fitted CL spectrum of the undoped zirconia powder.

Similarly is unclear which could be the luminescence center of the reported band around 400 nm (Z2 and A2 respectively in Figures 5 and 6). Following the experimental results, the intensity of this band does not vary significantly except for the sample 4.5-YSZ. Therefore, we cannot exclude that this luminescence may arise from another impurity atoms, like carbon contamination in the SEM vacuum chamber or synthesis subproducts.

About the oxygen defect in ZrO_2 lattice, we first consider that the electron beam irradiation exceeds band-gap energy, creating a band-to-band excitation with a recombination mechanism that could involve one or two levels electron transition. The electron−hole recombination process is promoted by emission of radiation. All those infra-band-gap energy states around 1.77−3 eV from the conduction band are the responsible for the observed luminescence emission.

Usually, the normal states are two electrons occupied for both this traps, but in the case that one electron is removed the remaining one is strongly localized because the states lie near the middle of zirconia band gap. The positively attractive field of this charged defect can easily trap one electron, forming the F^0 center. As reported by different authors, the relaxation process results in the luminescence emission centered around 430−460 nm.[20,38] In this case, according to the present fitting procedure, we found the major sub-band contribute around 485 nm. Considering that no dopant is present and the hafnia impurities generate a high wavelength luminescence, we should attribute this band to the intradefect transition in F^+ center, even though it is shifted respect to the mentioned reference. An explanation for this behavior could be probably a size-related effect, where the macroscopic crystal shows a similar luminescence compared to the microcrystal, but at different emission wavelength.[39] The other relevant CL sub-bands (Z4 and Z5) can eventually be ascribed to a slightly different set of defects, which could be F centers in a different structural location. According to Smits et al.,[18] one possibility to describe the CL spectral bands in zirconia is to take into account a different set of Zr−O bonds, which differs in bond length and in coordination number, in the presence of the oxygen vacancy. These authors already suggested that the defect luminescence in both pure and doped ZrO_2 could arise from lattice cells distorted by the presence of oxygen vacancy. If this is the case, the oxygen vacancy present in the structure should thus be very sensitive to the distortion of the oxygen sublattice, forming a quasi-continuum of defective energy states.

The fact that Y-doped zirconia series presents quite similar CL spectra compared to the undoped zirconia, as shown in Figure 6a−f, could be evidence that the radiative centers of undoped and Y^{3+}-doped ZrO_2 are basically the same. The luminescence of Y-doped zirconia defects was extensively studied by many research groups,[20,27] reporting that this system presents at least three kinds of defects: an intrinsic oxygen vacancy (F center) and to two different extrinsic oxygen vacancy complexes capable to coordinate one or two Y^{3+} atoms (i.e., the F_A and F_{AA} centers, respectively), able to produce three distinct luminescence bands positioned at 460, 550, and 600 nm. In the collected CL spectra from YSZ series is still possible to ascribe the bands A4 and A5 to the different color centers in the case of coordination with Y^{3+}. The newly formed F center in the case of yttria doping replaces the intrinsic F center, and reasonably the electronic levels of these oxygen vacancies in the YSZ system will not be found at the same energy values as in the case of undoped zirconia.

This could be mainly due because during the annealing treatment at high temperature, as well during the measurement under vacuum conditions, the mobility of the doubly ionized

dx.doi.org/10.1021/jp506923p | J. Phys. Chem. A 2014, 118, 9828−9836

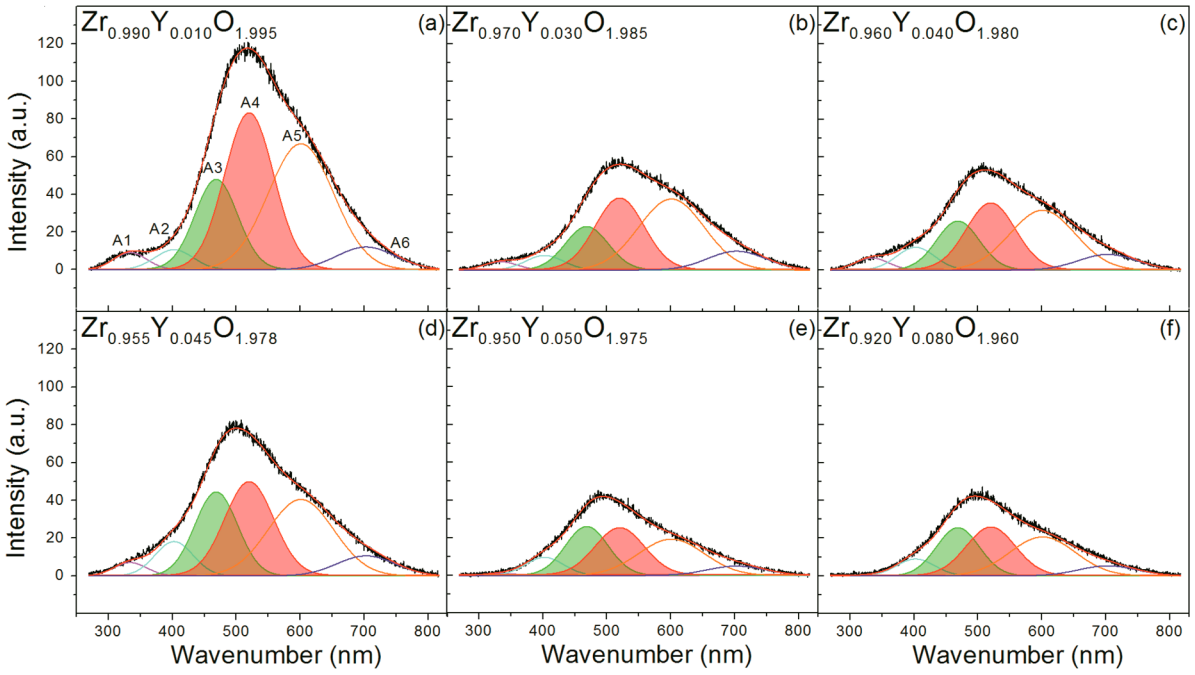

Figure 6. CL spectra and relative fitting collected for the sample 1-YSZ (a), 3-YSZ (b), 4-YSZ (c), 4.5-YSZ (d), 5-YSZ (e), and 8-YSZ (f).

Table 2. Position, FWMH, and Relative Area Weight of the Gaussian Band Set for Different Samples as Function of Dopant Content

			relative area weight (%)				
band	pos (nm)	FWMH (nm)	ZrO_2	1-YSZ	5-YSZ	8-YSZ	12-YSZ
(Z1) A1	(305) 334	(47) 61	(0.4)	2.5	3.4	0.4	0.5
(Z2) A2	(410) 402	(61) 70	(0.4)	3.3	7.5	7.7	8.8
(Z3) A3	(485) 469	(78) 79	(18.2)	17.2	18.4	25	27
(Z4) A4	(538) 520	(103) 90	(41.3)	34.3	28.6	28.9	29
(Z5) A5	(619) 601	(116) 120	(32.7)	36.6	34	30.7	28.6
(Z6) A6	(703) 703	(124) 107	(7)	5.8	7.8	7	5.8

oxygen vacancy (i.e., with formal charge +2) increased, promoting a migration toward the 3-fold-coordinated yttrium that presents a virtual negative charge compared to the 4-fold zirconium atoms. In this way, the complex Y^{3+}–V_O, in which usually the oxygen vacancy is founded to be occupying a next-nearest-neighbor site, is formed. For the electrical neutrality, the vacancy in this position cannot trap two electrons as in the case of undoped zirconia. Nevertheless, the luminescence mechanism must follow the two-step recombination process already mentioned above, even though it will be less efficient because of the unfavorite geometry position of the color center, being affected by the negative charge of the Y^{3+}. The reduced efficiency of the trap is clearly shown with the decreasing of the intensity as can be seen in Figure 5a–f.

In the context of a comparison between fully monoclinic polymorphs, and the fully tetragonal one (i.e., cf. Figures 4a and 4c), another difference resides in the presence of a low-wavelength peak located at around 330 nm (labeled A1). This emission has already been reported Wang et al.[40] for different thermal treatments of zirconia. The authors ascribed this band emission to a recombination process between electrons in an oxygen vacancy with deep depth with holes. In our case this band seems to be present relevantly only if two conditions are met: Y^{3+} is added, and the monoclinic polymorph exists in the sample. Therefore, this band has a weak emission in the undoped zirconia and in the YSZ samples with >5 at. % Y_2O_3. The intensity of the sub-band located at 330 nm does not vary significantly with increasing Y^{3+} content, as far as the monoclinic polymorph is preserved. It might arise from an oxygen-vacancy complex involving Y^{3+} and only detectable in the monoclinic polymorph due to its lower band gap as compared to the tetragonal one.[41]

4.3. Polymorphic Fractions in the Scanning Electron Microscope. The morphology of the CL spectrum of different YSZ systems was investigated in order to extract quantitative information on their polymorphic fractions. We already mentioned that, during the synthesis of the various YSZ systems, different ratios of monoclinic and tetragonal phases were produced. The overall intensity of the CL spectra gradually decreased with increasing dopant concentration, thus showing a "quenching" effect with Y^{3+} addition. In the attempt to understand which information we could actually extract from this systematic screening of CL spectra, we focused our attention on the ratio of the A4 to the A3 sub-band areas (i.e., henceforth referred to as $R = A_4/A_3$). This choice was suggested by the clear phenomenological relationship that this parameter showed to the overall morphology of the CL spectrum. Building upon the hint that the luminescence center could be related to the distortion of the oxygen sublattice, we plotted the normalized ratio $R = A_4/A_3$ and the c lattice cell

dx.doi.org/10.1021/jp506923p | J. Phys. Chem. A 2014, 118, 9828–9836

parameter as experimentally obtained from XRD data, as a function of the Y^{3+} dopant concentration. The lattice parameter was calculated as the weighted average of the monoclinic and tetragonal ones. The results are shown in Figure 7a–c.

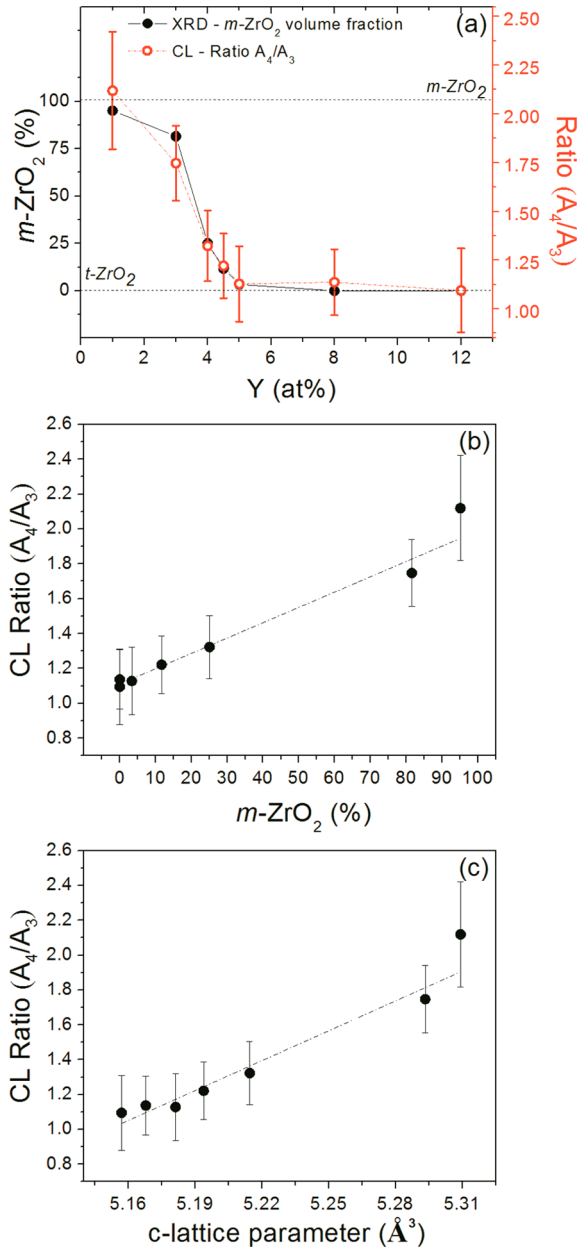

Figure 7. Comparison between the monoclinic volume fraction (calculated from XRD analysis (black, solid) and the A_4/A_3 ratio obtained by CL (red, dotted) as a function of Y^{3+} dopant concentration (a). Dependence of CL ratio with monoclinic volume fraction (b) and average *c*-lattice parameter (c). Each point is the average of 20 collected spectra.

The similarity of the two plots shown in Figure 7a and, thus, the dependence of the CL spectrum morphology on the dimension of the lattice cell (and its symmetry) appear evident (Figure 7b,c). With a linear fitting procedure a phenomenological equation can be then retrieved, which relates the monoclinic volume fraction and the lattice cell average volume to the parameter $R = A_4/A_3$ as follows:

$$R = 1.11 + 0.009V_m \quad (2)$$

where V_m expresses the monoclinic volume fraction.

While this is clear evidence that oxygen defects in both undoped zirconia and YSZ are strongly structural dependent, the overall luminescence intensity exhibits a strong decrease passing from the monoclinic to the tetragonal symmetry. However, once the polymorph population becomes fully tetragonal in the sample, even if the amount of oxygen vacancy in the system is progressively increasing, there seems to be no rationale in explaining the difference in the overall CL intensity of different tetragonal structures (i.e., 5-, 8-, and 12-YSZ). On the other hand, the relative intensity ratio $R = A_4/A_3$ seems capable to read to a degree of precision the tetragonal-to-monoclinic polymorphic ratio. A plausible explanation of such complicated set of data could be given as explained in the following. We cannot exclude that the reason for luminescence quenching in fully tetragonal YSZ samples could be a nonradiative and competitive recombination path involving both holes and electrons, which we have referred to as the "charge-trap hypothesis" in section 2. Since oxygen vacancy is a deep trap for electrons, the intensity reduction might be due to electron trapping at the oxygen vacancy followed by a nonradiative recombination. Theoretical calculations and EPR measurements have already shown that the complex consisting of an O ion coordinated with an Y^{3+} could be effective as a holes trap.[42,43] However, this can explain neither the drastic reduction in overall CL intensity with passing from the monoclinic to the tetragonal polymorph nor the increase in the concentration of F_{AA} centers over that of F_A centers, as clearly detected here. Moreover, one would expect that the monoclinic structure, with less overcrowding of oxygen, should have less strain as compared to the tetragonal one. This is in contrast with the so-called lattice-strain hypothesis as so far stated by other authors. It is actually the relaxed monoclinic lattice that emits with higher efficiency. On the basis of this evidence, we believe that it is the presence of Y^{3+} itself, rather than lattice strain, which is responsible for the observed quenching phenomenon. In other words, the intrinsic vacancies present in the undoped lattice are the most efficient because they trap two electrons to gain electrical neutrality. However, as soon as Y^{3+} ions are introduced in the system, those intrinsic vacancies migrate to Y-sites in next-nearest-neighbor locations, namely in a less efficient lattice location. This phenomenon is tentatively referred to as "delocalization" of vacancy sites. Given the quite low efficiency of Y^{3+}-related vacancies, a newly formed vacancy population due to an increasing addition of Y_2O_3 fails in compensating for the loss of CL emission associated with the annihilation of intrinsic vacancies. The overall intensity of the CL emission is thus dominated by an annihilation process of intrinsic vacancies rather than by the increasingly new formation of Y^{3+}-related vacancy sites.

As an application of the assessment of monoclinic-to-tetragonal ratio in YSZ by CL analysis, we analyzed the polymorphic fraction in an autoclave-exposed 3 mol % YSZ bulk sample, which was partially damaged (with surface exfoliation) under the effect of hydrothermal loading. In order to confirm the validity of the polymorphic fraction measurement by CL in the SEM, we selected a profile on the investigated area, and compared measurements by confocal Raman spectroscopy, as shown in Figure 8a. Figure 8b shows a SEM micrograph and a CL map of the monoclinic fraction (i.e., according to eq 1). The good agreement between the values

dx.doi.org/10.1021/jp506923p | J. Phys. Chem. A 2014, 118, 9828–9836

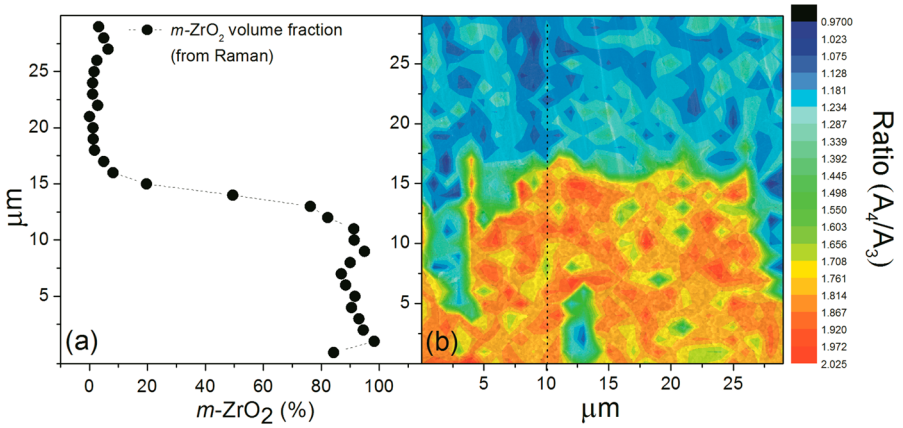

Figure 8. Calculated monoclinic volume fraction from Raman using eq 1 (a) along the dotted line reported in (b). Part b shows a 30 × 30 CL map overlapped to the SEM micrographs on the same location, in which colors express the CL ratio values from blue $R \sim 1$ to red $R \sim 2$, showing respectively the tetragonal and monoclinic polymorphic distribution.

obtained by the two different techniques indicates that indeed phase-fraction assessments in the SEM are feasible. The main advantage in performing these assessments by CL rather than by Raman spectroscopy might reside in the higher spatial resolution achievable by using electrons instead than laser irradiation as an excitation source.

5. CONCLUSION

In this paper, we aimed at analyzing some physical chemistry aspects of the CL emission from undoped and Y-doped zirconia lattices. Clear evidence have been obtained for linking the morphology of the CL emission spectra to the lattice cell volume obtained by XRD experiments. This opened the way to build up a phenomenological equation that enables the quantitative assessment of polymorphic fractions in the SEM. Some new aspects were unveiled for zirconia emission and for the role of small amounts of Y^{3+} dopant in its lattice. From this body of new physical evidence, it vividly appears how important is the role that oxygen off-stoichiometry plays in the physicochemical behavior of the ZrO_2 surfaces. CL spectroscopy proved thus quite innovative in this context, allowing one to discuss the presence of point defects and, through them, to map polymorphic fractions in the SEM.

AUTHOR INFORMATION

Corresponding Author

*E-mail: pezzotti@kit.ac.jp (G.P.).

Notes

The authors declare no competing financial interest.

REFERENCES

(1) Thamaraiselvi, T.; Rajeswari, S. Biological evaluation of bioceramic materials - A review. *Trends Biomater. Artif. Organs* **2004**, *18*, 9−17.

(2) Pezzotti, G. *Advanced Materials for Joint Implants*; Pan Stanford: Singapore, 2013.

(3) Pezzotti, G.; Yamamoto, K. Artificial hip joints: The biomaterials challenge. *J. Mech. Behav. Biomed.* **2014**, *31*, 3−20.

(4) Kim, Y.-I.; Woodward, P. M.; Baba-Kishi, K. Z.; Tai, C. W. Characterization of the structural, optical, and dielectric properties of oxynitride perovskites AMO_2N (A = Ba, Sr, Ca; M = Ta, Nb). *Chem. Mater.* **2004**, *16*, 1267−1276.

(5) Nguyen, T. L.; Kobayashi, K.; Honda, T.; Iimura, Y.; Kato, K.; Neghisi, A.; Nozaki, K.; Tappero, F.; Sasaki, K.; Shirahama, H.; et al. Preparation and evaluation of doped ceria interlayer on supported stabilized zirconia electrolyte SOFCs by wet ceramic processes. *Solid State Ionics* **2004**, *174*, 163−174.

(6) Fuertes, A. Synthesis and properties of functional oxynitrides - from photocatalysts to CMR materials. *Dalton. Trans.* **2010**, *39*, 5942−5948.

(7) Fukatsu, K.; Leto, A.; Zhu, W. L.; Sugano, N.; Pezzotti, G. Kinetics and the role of off-stoichiometry in the environmentally driven phase transformation of commercially available zirconia femoral heads. *Acta Biomater.* **2012**, *8*, 1639−1647.

(8) Leto, A.; Zhu, W.; Matsubara, M.; Pezzotti, G. Bioinertness and fracture toughness evaluation of the monoclinic zirconia surface film of oxinium femoral head by Raman and cathodoluminescence spectroscopy. *J. Mech. Behav. Biomed.* **2014**, *31*, 135−144.

(9) Pezzotti, G.; Leto, A. Contribution of spatially and spectrally resolved cathodoluminescence to study crack-tip phenomena in silica glass. *Phys. Rev. Lett.* **2009**, *103*, 175501.

(10) Pezzotti, G.; Hosokawa, K.; Munisso, M. C.; Leto, A.; Zhu, W. Stress dependence of optically active diamagnetic point defects in silicon oxynitride. *J. Phys. Chem. A* **2007**, *111*, 8367−8373.

(11) Boffelli, M.; Back, M.; Cattaruzza, E.; Gonella, F.; Trave, E.; Leto, A.; Glisenti, A.; Pezzotti, G. Off-stoichiometry spectroscopic investigations of pure amorphous silica and N-doped silica thin films. *J. Phys. Chem. C* **2013**, *117*, 3475−3482.

(12) Pezzotti, G.; Munisso, M. C.; Lessnau, K.; Zhu, W. Quantitative assessments of residual stress fields at the surface of alumina hip joints. *J. Biomed. Mater. Res., Part B* **2010**, *95B*, 250−262.

(13) Pezzotti, G.; Munisso, M. C.; Porporati, A. A.; Lessnau, K. On the role of oxygen vacancies and lattice strain in the tetragonal to monoclinic transformation in alumina/zirconia composites and improved environmental stability. *Biomaterials* **2010**, *31*, 6901−6908.

(14) Garvie, R. C. Stabilization of the tetragonal structure in zirconia microcrystals. *J. Phys. Chem.* **1978**, *82*, 218−224.

(15) Garvie, R. C. The occurrence of metastable tetragonal zirconia as a crystallite size effect. *J. Phys. Chem.* **1965**, *69*, 1238−1243.

(16) Cheng, Y.-B.; Thompson, D. P. Role of anion vacancies in nitrogen-stabilized zirconia. *J. Am. Ceram. Soc.* **1993**, *76*, 683−688.

(17) Smits, K.; Grigorjeva, L.; Łojkowski, W.; Fidelus, J. D. Luminescence of oxygen related defects in zirconia nanocrystals. *Phys. Status Solidi C* **2007**, *4*, 770−773.

(18) Smits, K.; Grigorjeva, L.; Millers, D.; Sarakovskis, A.; Grabis, J.; Lojkowski, W. Intrinsic defect related luminescence in ZrO_2. *J. Lumin.* **2011**, *131*, 2058−2062.

(19) Yueh, H. K.; Cox, B. Luminescence properties of zirconium oxide films. *J. Nucl. Mater.* **2003**, *323*, 57−67.

(20) Petrik, N. G.; Taylor, D. P.; Orlando, T. M. Laser-stimulated luminescence of yttria-stabilized cubic zirconia crystals. *J. Appl. Phys.* **1999**, *85*, 6770−6776.

(21) Devanathan, R.; Weber, W. J.; Singhal, S. C.; Gale, J. D. Computer simulation of defects and oxygen transport in yttria-stabilized zirconia. *Solid State Ionics* **2006**, *177*, 1251−1258.
(22) Goff, J. P.; Hayes, W.; Hull, S.; Hutchings, M. T.; Clausen, K. N. Defect structure of yttria-stabilized zirconia and its influence on the ionic conductivity at elevated temperatures. *Phys. Rev. B* **1999**, *59*, 14202−14219.
(23) Vonk, V.; Khorshidi, N.; Stierle, A.; Dosch, H. Atomic structure and composition of the yttria-stabilized zirconia (111) surface. *Surf. Sci.* **2013**, *612*, 69−76.
(24) Čížek, J.; Melikhova, O.; Procházka, I.; Kuriplach, J.; Kužel, R.; Brauer, G.; Anwand, W.; Konstantinova, T. E.; Danilenko, I. A. Defect studies of nanocrystalline zirconia powders and sintered ceramics. *Phys. Rev. B* **2010**, *81*, 024116.
(25) Ding, H.; Virkar, A. V.; Liu, F. Defect configuration and phase stability of cubic versus tetragonal yttria-stabilized zirconia. *Solid State Ionics* **2012**, *215*, 16−23.
(26) Fidelus, J. D.; Lojkowski, W.; Millers, D.; Smits, K.; Grigorjeva, L. In *Advanced Nanocrystalline ZrO_2 for Optical Oxygen Sensors*; IEEE: 2009; pp 1268−1272.
(27) Nakajima, H.; Mori, T. Photoluminescence excitation bands corresponding to defect states due to oxygen vacancies in yttria-stabilized zirconia. *J. Alloys Compd.* **2006**, *408*, 728−731.
(28) Marin, R.; Sponchia, G.; Zucchetta, E.; Riello, P.; Enrichi, F.; De Portu, G.; Benedetti, A. Monitoring the t-m martensitic phase transformation by photoluminescence emission in Eu^{3+}-doped zirconia powders. *J. Am. Ceram. Soc.* **2013**, *96*, 2628−2635.
(29) Riello, P.; Canton, P.; Fagherazzi, G. Quantitative phase analysis in semicrystalline materials using the Rietveld method. *J. Appl. Crystallogr.* **1998**, *31*, 78−82.
(30) Katagiri, G.; Ishida, H.; Ishitani, A.; Masaki, T. Direct determination by a Raman microprobe of the transformation zone size in Y_2O_3 containing tetragonal ZrO_2 polycrystals. *Adv. Ceram.* **1986**, *24*, 537−544.
(31) Kim, B. K.; Hamaguchi, H. O. Mode assignments of the Raman spectrum of monoclinic zirconia by isotopic exchange technique. *Phys. Status Solidi B* **1997**, *203*, 557−563.
(32) Viazzi, C.; Bonino, J. P.; Ansart, F.; Barnabe, A. Structural study of metastable tetragonal YSZ powders produced via a sol-gel route. *J. Alloys Compd.* **2008**, *452*, 377−383.
(33) Arora, A. K.; Rajalakshmi, M.; Ravindran, T. R.; Sivasubramanian, V. Raman spectroscopy of optical phonon confinement in nanostructured materials. *J. Raman Spetrosc.* **2007**, *38*, 604−617.
(34) Campbell, I. H.; Fauchet, P. M. The effects of microcrystal size and shape on the one phonon Raman spectra of crystalline semiconductors. *Solid State Commun.* **1986**, *58*, 739−741.
(35) Hur, J.-H.; Park, S.; Chung, U.-I. First principles study of oxygen vacancy states in monoclinic ZrO_2: Interpretation of conduction characteristics. *J. Appl. Phys.* **2012**, *112*, 113719.
(36) Kirm, M.; Aarik, J.; Jürgens, M.; Sildos, I. Thin films of HfO_2 and ZrO_2 as potential scintillators. *Nucl. Instrum. Methods Phys. Res., Sect. A* **2005**, *537*, 251−255.
(37) Kiisk, V.; Lange, S.; Utt, K.; Tätte, T.; Mändar, H.; Sildos, I. Photoluminescence of sol−gel-prepared hafnia. *Physica B: Condens. Matter* **2010**, *405*, 758−762.
(38) Korsunska, N.; Papusha, V.; Kolomys, O.; Strelchuk, V.; Kuchuk, A.; Kladko, V.; Bacherikov, Y.; Konstantinova, T.; Khomenkova, L. Nanostructured Y-doped ZrO_2 powder: peculiarities of light emission under electron beam excitation. *Phys. Status Solidi C* **2014**, 1610−1642.
(39) Smits, K.; Millers, D.; Grigorjeva, L.; Fidelus, J. D.; Lojkowski, W. Comparison of ZrO_2:Y nanocrystals and macroscopic single crystal luminescence. *J. Phys. Conf. Ser.* **2007**, *93*, 012035.
(40) Wang, Z.; Zhang, J.; Zheng, G.; Liu, Y.; Zhao, Y. The unusual variations of photoluminescence and afterglow properties in monoclinic ZrO_2 by annealing. *J. Lumin.* **2012**, *132*, 2817−2821.
(41) Garcia, J. C.; Scolfaro, L. M. R.; Lino, A. T.; Freire, V. N.; Farias, G. A.; Silva, C. C.; Alves, H. W. L.; Rodrigues, S. C. P.; da Silva, E. F. Structural, electronic, and optical properties of ZrO_2 from ab initio calculations. *J. Appl. Phys.* **2006**, *100*, 104103.
(42) Azzoni, C. B.; Bolis, L.; Paleari, A.; Samoggia, G.; Scardina, F. Disorder-induced optical and paramagnetic properties in zirconium dioxide: Role of low-symmetry crystal fields. *Phys. Rev. B* **1995**, *51*, 15942−15946.
(43) Azzoni, C. B.; Paleari, A. Sevenfold- and sixfold-coordinated Zr^{3+} ions in cubic stabilized zirconia: Crystal-field approach. *Phys. Rev. B* **1991**, *44*, 6858−6863.